

New physics searches with $b \rightarrow s\ell^+\ell^-$ transitions and rare decays at LHCb

K. DE BRUYN on behalf of the LHCb COLLABORATION

Aix Marseille Univ, CNRS/IN2P3, CPPM - Marseille, France

received 16 September 2017

Summary. — Several tensions between the experimental measurements and their Standard Model predictions have been observed in rare B meson decays mediated by $b \rightarrow s\ell^+\ell^-$ transitions. To understand the nature of these discrepancies, the LHCb experiment is extending its previously reported studies with additional observables and decay modes. These proceedings summarise the latest results on the topic. They report on a measurement of the interference between the long- and short-distance contributions in $B^+ \rightarrow K^+\mu^+\mu^-$ decays, on the searches for the $B \rightarrow \mu^+\mu^-\mu^+\mu^-$ and $B \rightarrow \tau^+\tau^-$ decays, and present an update of the $B \rightarrow \mu^+\mu^-$ analysis, which includes the first measurement of the $B_s^0 \rightarrow \mu^+\mu^-$ effective lifetime.

1. – Introduction

Rare B meson decays that are mediated by $b \rightarrow s\ell^+\ell^-$ transitions offer powerful probes to search for beyond the Standard Model physics. In the Standard Model (SM), these flavour changing neutral currents are forbidden at tree level and can therefore only proceed via loop topologies, suppressing their branching fractions. New physics (NP) models, on the other hand, can introduce couplings to new (heavy) mediators at both the tree and loop level. Measurements of the branching fractions and angular observables in these decays allow us to probe the NP effects, which are often associated with energy scales much higher than those accessible by direct searches.

In the past years, several tensions between the experimental measurements and their SM predictions have been observed in $b \rightarrow s\ell^+\ell^-$ transitions. Most notably, these include the measurements of the angular observables in $B^0 \rightarrow K^{*0}\mu^+\mu^-$ [1-3], and the ratio R_K between the branching fractions of the $B^+ \rightarrow K^+\mu^+\mu^-$ and $B^+ \rightarrow K^+e^+e^-$ decays [4], which forms a stringent test of lepton flavour universality. In addition, many differential branching fractions in $b \rightarrow s\mu^+\mu^-$ decays are found to be systematically below their SM expectations [5-7]. Although individually these measurements do not yet provide sufficient evidence for NP, combined model-independent analyses using the effective field

theory framework point towards a deviation from the SM value for the Wilson coefficient C_9 by four to five standard deviations [8-10].

To understand the nature of this discrepancy, be it SM or NP, it is not only important to confront the existing analyses with additional data, but also to extend the studies with additional observables and decay modes. These proceedings summarise the latest results on the topic. They report on a measurement of the interference between the long- and short-distance contributions in $B^+ \rightarrow K^+ \mu^+ \mu^-$ decays (sect. 2), on the searches for the $B \rightarrow \mu^+ \mu^- \mu^+ \mu^-$ (sect. 3) and $B \rightarrow \tau^+ \tau^-$ decays (sect. 5), and present an update of the $B \rightarrow \mu^+ \mu^-$ analysis (sect. 4). Throughout these proceedings B refers to either a B^0 or a B_s^0 meson, and the inclusion of charge-conjugate processes is implied. Except for the updated $B \rightarrow \mu^+ \mu^-$ analysis, which also includes data from Run 2 of the LHC, the measurements are performed on a data set corresponding to 3 fb^{-1} of integrated luminosity collected by the LHCb experiment in 2011 and 2012.

2. – Resonance effects in $B^+ \rightarrow K^+ \mu^+ \mu^-$ decays

Underestimated long-distance charm-loop effects could offer a SM explanation for the tension observed in the dimuon mass squared, q^2 , distribution of the angular observable P'_5 measured in $B^0 \rightarrow K^{*0} \mu^+ \mu^-$ decays [1]. If they indeed account for the current discrepancies between the data and the SM predictions, such contributions need to be sizeable in dimuon mass regions far from the pole masses of the J/ψ and $\psi(2S)$ resonances. It is thus important to understand how well such effects are modelled in the SM and how they interfere with the short-distance contributions in these q^2 regions. LHCb has therefore performed a study of the $B^+ \rightarrow K^+ \mu^+ \mu^-$ decay channel, measuring for the first time the phase difference between the short-distance and narrow-resonance amplitudes.

The short-distance contributions to the CP -averaged differential decay rate of the $B^+ \rightarrow K^+ \mu^+ \mu^-$ decay originate from electroweak penguin topologies, and can be parametrised following the notation of ref. [11] as

$$(1) \quad \frac{d\Gamma}{dq^2} = \frac{G_F^2 \alpha^2 |V_{tb} V_{ts}^*|^2}{128\pi^5} |k| \beta \left\{ \frac{2}{3} |k|^2 \beta^2 |C_{10} f_+(q^2)|^2 + \frac{4m_\mu^2(m_B^2 - m_K^2)^2}{q^2 m_B^2} |C_{10} f_0(q^2)|^2 \right. \\ \times |k|^2 \left[1 - \frac{1}{3} \beta^2 \right] \left| C_9 f_+(q^2) + 2C_7 \frac{m_b + m_s}{m_B + m_K} f_T(q^2) \right|^2 \left. \right\}.$$

Here G_F , α and V_{ij} are respectively the Fermi constant, the QED fine-structure constant and the relevant CKM matrix elements; $|k|$ is the kaon momentum in the B^+ meson rest frame; $\beta^2 = 1 - 4m_\mu^2/q^2$; m_s , m_b , m_μ , m_K and m_B are the respective particle masses; $f_{0,+,\text{T}}$ represent the scalar, vector and tensor $B \rightarrow K$ form factors; and $C_{7,9,10}$ denote the Wilson coefficients associated with the electromagnetic dipole operator, the vector current and the axial-vector current. The corresponding right-handed operators, which are suppressed in the SM, are ignored in this analysis. The coefficient C_7 is fixed to its SM value, taken from ref. [12], while C_9 and C_{10} are free parameters in the fit.

In contrast to previous analyses, the long-distance amplitudes associated with vector resonances in the dimuon mass spectrum are also modelled explicitly. They are taken into account by introducing an effective Wilson coefficient replacing C_9 in eq. (1),

$$(2) \quad C_9^{\text{eff}} = C_9 + \sum_j \eta_j e^{i\delta_j} A_j^{\text{res}}(q^2),$$

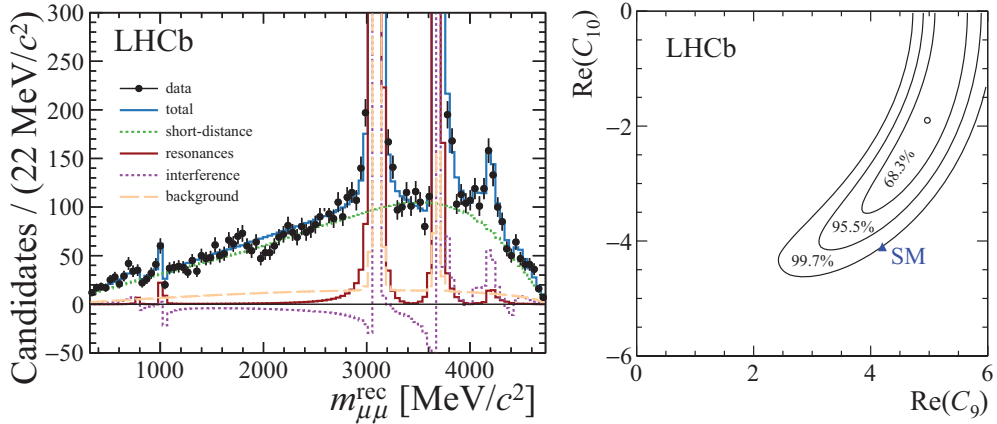


Fig. 1. – Left: fit to the dimuon mass distribution of the $B^+ \rightarrow K^+ \mu^+ \mu^-$ events. Shown is the solution for which both the J/ψ and $\psi(2S)$ have a negative sign. Right: two-dimensional likelihood profile for the Wilson coefficients C_9 and C_{10} .

where η_j is the magnitude of the resonance and δ_j its phase relative to C_9 . The sum j includes the ρ , ω , ϕ , J/ψ , $\psi(2S)$ as well as the broad charmonium states above the open charm threshold. Their amplitudes A_j^{res} are modelled using Breit-Wigner functions, and, with the exception of the J/ψ and $\psi(2S)$, their widths and pole masses are fixed to the known values.

The fit to the dimuon mass spectrum has a four-fold degenerate solution, corresponding to remaining ambiguities in the signs of the J/ψ and $\psi(2S)$ phases. The values of these phases are compatible with $\pm \frac{1}{2}$, which implies that the interference with the non-resonant penguin contributions is small, disfavouring this effect as an explanation for the tensions in P'_5 . The solution for which both the J/ψ and $\psi(2S)$ have a negative sign is shown in the left panel of fig. 1, while the other three solutions can be found in ref. [13], together with the numerical results of the fit. The two-dimensional likelihood profile for C_9 and C_{10} is shown in the right panel of fig. 1, preferring the solution $|C_9| > |C_9^{\text{SM}}|$ and $|C_{10}| < |C_{10}^{\text{SM}}|$. Alternatively, if C_{10} is constrained to its SM value, then the fit prefers $|C_9| < |C_9^{\text{SM}}|$, in agreement with the global fits [8-10]. The branching fraction of the short-distance component can be obtained by integrating eq. (1), giving [13]

$$(3) \quad \mathcal{B}(B^+ \rightarrow K^+ \mu^+ \mu^-) = (4.37 \pm 0.15 \text{ (stat)} \pm 0.23 \text{ (syst)}) \times 10^{-7}.$$

Note that unlike the previous, binned measurement [5], which reports compatible results, this branching fraction does not rely on an extrapolation over the excluded q^2 region.

3. – Search for $B \rightarrow \mu^+ \mu^- \mu^+ \mu^-$ decays

A search for the decay of a neutral B meson into four muons is performed, improving the existing branching fraction limits [14] for two specific scenarios: the non-resonant SM amplitude and a supersymmetry model where the decay proceeds through a scalar S and a pseudo-scalar P sgoldstino particle. The main contribution to the SM amplitude originates from the $B \rightarrow \mu^+ \mu^-$ electroweak loop topologies in combination with a virtual photon, from which the other muon pair is created. The NP model is motivated by the

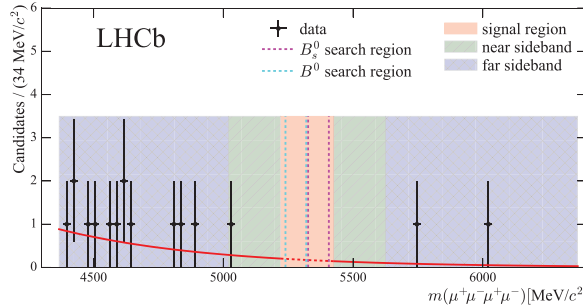


Fig. 2. – Mass distribution of the selected $\mu^+\mu^-\mu^+\mu^-$ events. The coloured boxes define the various signal and control regions used in the analysis.

result from the HyperCP experiment, which found an excess of events in the dimuon mass spectrum of the $\Sigma^+ \rightarrow p\mu^+\mu^-$ decay channel that is consistent with the decay of a resonance $P \rightarrow \mu^+\mu^-$ with a mass $m_P = (214.3 \pm 0.5)$ MeV/ c^2 [15]. A dedicated search for the $B \rightarrow S(\rightarrow \mu^+\mu^-)P(\rightarrow \mu^+\mu^-)$ decay, assuming masses for the sgoldstino particles of $m_S = 2.6$ GeV/ c^2 and $m_P = 214.3$ MeV/ c^2 , is therefore performed.

The resonant SM amplitudes are reduced to a negligible level by vetoing the contributions from the ϕ , J/ψ and $\psi(2S)$ in all $\mu^+\mu^-$ -pair combinations. Backgrounds arising from $\pi \rightarrow \mu$ mis-identification are suppressed by imposing particle identification (PID) requirements, and a MatrixNet multivariate classifier [16] based on a Boosted Decision Tree (BDT) is used against the combinatorial background. The selection requirements on the PID and MatrixNet classifier are optimised using the near sideband region in data, defined using the four-muon mass distribution as illustrated in fig. 2.

The expected yield for the remaining background in the signal region is extrapolated from a fit to the far sideband, resulting in 0.47 ± 0.29 (0.55 ± 0.31) expected events in the B_s^0 (B^0) search window. No events are observed inside these two regions and a limit is therefore set on the branching fractions, giving [17]

$$(4) \quad \mathcal{B}(B^0 \rightarrow \mu^+\mu^-\mu^+\mu^-) < 6.9 \times 10^{-10} @ 95\% \text{ C.L.},$$

$$(5) \quad \mathcal{B}(B_s^0 \rightarrow \mu^+\mu^-\mu^+\mu^-) < 2.5 \times 10^{-9} @ 95\% \text{ C.L.},$$

$$(6) \quad \mathcal{B}(B^0 \rightarrow S(\rightarrow \mu^+\mu^-)P(\rightarrow \mu^+\mu^-)) < 6.0 \times 10^{-10} @ 95\% \text{ C.L.},$$

$$(7) \quad \mathcal{B}(B_s^0 \rightarrow S(\rightarrow \mu^+\mu^-)P(\rightarrow \mu^+\mu^-)) < 2.2 \times 10^{-9} @ 95\% \text{ C.L.}.$$

The two-dimensional exclusion limits are shown in fig. 3.

4. – Branching fraction and effective lifetime measurements in $B \rightarrow \mu^+\mu^-$ decays

Since they are characterised by a purely leptonic final state, the time-integrated SM branching fractions of B meson decays into two charged muons, $\mathcal{B}(B^0 \rightarrow \mu^+\mu^-) = (1.06 \pm 0.09) \times 10^{-8}$ and $\mathcal{B}(B_s^0 \rightarrow \mu^+\mu^-) = (3.65 \pm 0.23) \times 10^{-7}$, can be predicted with small theoretical uncertainties [18]. This feature makes the $B \rightarrow \mu^+\mu^-$ decay channels sensitive probes to search for beyond the SM physics, and therefore key modes to search for and study at the LHC. This search culminated in the first observation of the $B_s^0 \rightarrow \mu^+\mu^-$ decay from a combined analysis of the LHCb and CMS Run 1 data [19].

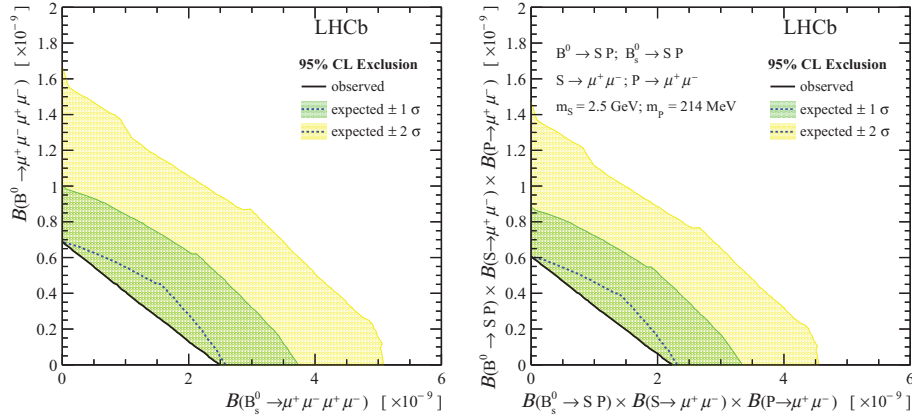


Fig. 3. – Two-dimensional 95% confidence level exclusion limits for the $B \rightarrow \mu^+\mu^-\mu^+\mu^-$ (left) and $B \rightarrow S(\rightarrow \mu^+\mu^-)P(\rightarrow \mu^+\mu^-)$ (right) searches.

LHCb has now updated its Run 1 analysis to include 1.4 fb^{-1} of integrated luminosity collected in 2015 and 2016 at a centre-of-mass energy of 13 TeV. In addition, several key aspects of the analysis have been revised and improved. These include new isolation variables, which aim to identify other tracks in the event that originate from the same b -hadron decay, a reoptimised BDT classifier, and more stringent PID requirements on the two muon candidates. Together, these improvements lead to a 50% better suppression of the combinatorial background. The different PID requirements lead to a 10% lower signal efficiency, but increase the rejection power for doubly mis-identified $B \rightarrow h^+h^{(\prime)-}$ modes, which form the most dangerous background, by 50%. Other partially reconstructed backgrounds, which potentially extend into the B^0 mass window, include B decays with two real muons, and b -hadron decays with one or more hadrons misidentified as muons. All partially reconstructed backgrounds are modelled and included in the fit. The dimuon mass distribution of the selected $B \rightarrow \mu^+\mu^-$ candidates with a BDT response greater than 0.5 is shown in fig. 4.

The $B \rightarrow \mu^+\mu^-$ branching fractions are determined from a simultaneous fit of the Run 1 and Run 2 data to the dimuon mass distribution of the selected candidates in the

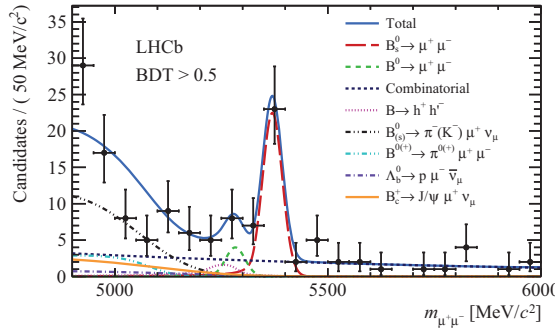


Fig. 4. – Mass distribution of the selected $B \rightarrow \mu^+\mu^-$ candidates with $\text{BDT} > 0.5$, with the result of the fit overlaid.

range [4900, 6000] MeV/c². The fit is performed in 4 bins of the BDT output, ignoring events with a BDT response below 0.25. The $B_s^0 \rightarrow \mu^+\mu^-$ decay is observed with a significance of 7.8 standard deviations, and a branching fraction [20]

$$(8) \quad \mathcal{B}(B_s^0 \rightarrow \mu^+\mu^-) = (3.0 \pm 0.6 \text{ (stat)}^{+0.3}_{-0.2} \text{ (syst)}) \times 10^{-9},$$

which is the first observation of this mode by a single experiment. Since the significance of the $B^0 \rightarrow \mu^+\mu^-$ signal is only 1.6 standard deviations, an upper limit is set on its branching fraction at [20]

$$(9) \quad \mathcal{B}(B^0 \rightarrow \mu^+\mu^-) < 3.4 \times 10^{-10} \quad @ 95\% \text{ C.L.}$$

The two-dimensional likelihood profile for the $B \rightarrow \mu^+\mu^-$ branching fractions is shown in fig. 5, showing that the best fit solution is in good agreement with the SM expectation.

The effective lifetime [21] offers a second probe to search for NP effects in $B_s^0 \rightarrow \mu^+\mu^-$ decays, complementing the branching fraction measurement. It can be used to constrain the mass-eigenstate-rate-asymmetry $\mathcal{A}_{\Delta\Gamma}$, which quantifies the relative contributions from the heavy and light mass-eigenstates of the B_s^0 meson system to the dimuon final state. The analysis is performed in two stages: First, weights are determined for the signal candidates based on a fit to the dimuon mass distribution. Afterwards, the decay time distribution of the weighted signal events is fitted with a single exponential, corrected for resolution and acceptance effects. To avoid contamination from partially reconstructed physics backgrounds as well as from the $B^0 \rightarrow \mu^+\mu^-$ component, the fitted mass range is reduced to [5300, 6000] MeV/c². The fit strategy has been validated on the $B^0 \rightarrow K^+\pi^-$ normalisation channel. For the $B_s^0 \rightarrow \mu^+\mu^-$ signal it gives [20]

$$(10) \quad \tau(B_s^0 \rightarrow \mu^+\mu^-) = 2.04 \pm 0.44 \text{ (stat)} \pm 0.05 \text{ (syst)} \text{ ps.}$$

The measurement is compatible with $\mathcal{A}_{\Delta\Gamma} = 1 (-1)$ at 1 (1.4) standard deviations.

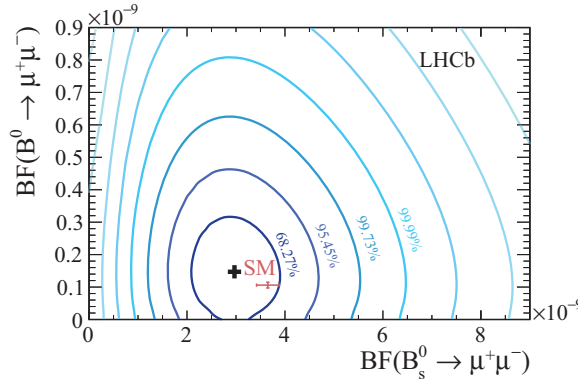


Fig. 5. – Two-dimensional likelihood profile for the $B^0 \rightarrow \mu^+\mu^-$ and $B_s^0 \rightarrow \mu^+\mu^-$ branching fractions.

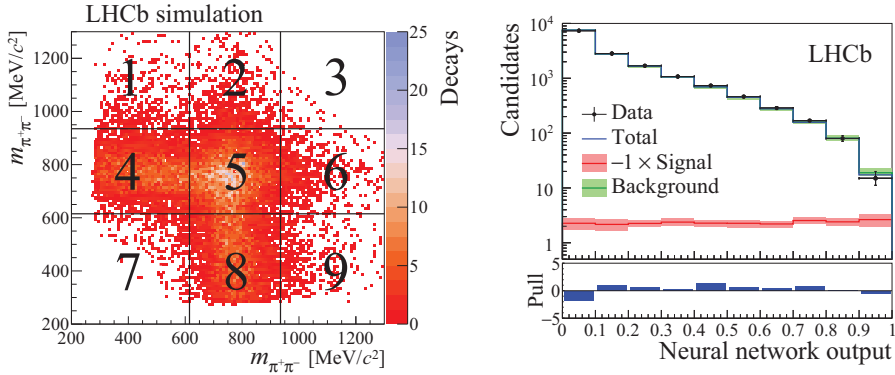


Fig. 6. – Left: two-dimensional distribution of the invariant masses $m_{\pi^+\pi^-}$ of the two oppositely charged two-pion combinations for simulated $B_s^0 \rightarrow \tau^+\tau^-$ candidates. The vertical and horizontal lines illustrate the sector boundaries. Right: distribution of the NN output in the signal region, with the result of the fit overlaid.

5. – Search for $B \rightarrow \tau^+\tau^-$ decays

Several NP explanations for the anomalies observed in $b \rightarrow s\ell^+\ell^-$ transitions predict enhanced branching fractions for the $B \rightarrow \tau^+\tau^-$ decays compared to their SM expectations [18], $\mathcal{B}(B^0 \rightarrow \tau^+\tau^-) = (2.22 \pm 0.19) \times 10^{-8}$ and $\mathcal{B}(B_s^0 \rightarrow \tau^+\tau^-) = (7.73 \pm 0.49) \times 10^{-7}$. The experimental search is, however, considerably more challenging than for their muonic counterparts discussed above due to the presence of at least two neutrinos in the final state.

LHCb has performed a search for the $B \rightarrow \tau^+\tau^-$ decays, where both τ leptons are reconstructed in the hadronic $\tau^- \rightarrow \pi^+\pi^-\pi^-\nu_\tau$ mode. The analysis exploits the intermediate resonances of the $\tau^- \rightarrow a_1^-(1260)\nu_\tau \rightarrow \rho^0(770)\pi^-\nu_\tau$ decay chain to define three regions in the data. These regions are identified using the two-dimensional distribution of the invariant masses $m_{\pi^+\pi^-}$ of the two oppositely charged two-pion combinations, which has been divided into nine sectors, as illustrated in the left panel of fig. 6. The signal region consists of B candidates with both τ candidates in sector 5, and is used to determine the signal yield. The signal-depleted region, composed of B candidates having at least one τ candidate in sectors 1, 3, 7 or 9, provides a sample used when optimising the selection. The control region corresponds to B candidates with one τ candidate in sectors 4, 5 or 8 and the other in sectors 4 or 8, and provides the background model. The signal selection is based on a two-stage neural network (NN) classifier using kinematic, topological and isolation variables. After the selection, the signal, signal-depleted, and control regions contain 16, 13 and 58% of the simulated signal candidates, respectively. The corresponding fractions of selected candidates in data are 7, 37, and 47%. Most of the signal decays thus fall into the control region, but the signal region, which contains about 14700 candidates in data after the full selection, is the most sensitive due to the low background contamination.

The signal yield is obtained from a binned maximum likelihood fit to a NN output, in which the signal model is taken from the $B \rightarrow \tau^+\tau^-$ simulation while the background

model is taken from the data control region, subtracting the signal contribution. The fit model can be written as:

$$(11) \quad \text{NN}_{\text{data}}^{\text{SR}} = s \times \widehat{\text{NN}}_{\text{sim}}^{\text{SR}} + f_b \times \left(\text{NN}_{\text{data}}^{\text{CR}} - s \cdot \frac{\epsilon^{\text{CR}}}{\epsilon^{\text{SR}}} \widehat{\text{NN}}_{\text{sim}}^{\text{CR}} \right)$$

where $\text{NN}_{\text{sim}/\text{data}}^{\text{SR}}$ ($\text{NN}_{\text{sim}/\text{data}}^{\text{CR}}$) is the NN distribution in the signal (control) region from simulation/data, s is the signal yield, f_b is the scale factor for the background template, and ϵ^{SR} (ϵ^{CR}) is the signal efficiency in the signal (control) region. The $\widehat{\cdot}$ represents normalised distributions. The result of the fit to data [22] is shown in the right panel of fig. 6 and gives a signal yield $s = -23^{+63}_{-53}(\text{stat})^{+41}_{-40}(\text{syst})$, consistent with the background-only hypothesis.

Assuming no contribution from $B^0 \rightarrow \tau^+\tau^-$ decays, an upper limit is set on the branching fraction [22]

$$(12) \quad \mathcal{B}(B_s^0 \rightarrow \tau^+\tau^-) < 6.8 \times 10^{-3} \quad @ 95\% \text{ C.L. .}$$

This is the first limit on the $B_s^0 \rightarrow \tau^+\tau^-$ mode. If instead, no contribution from $B_s^0 \rightarrow \tau^+\tau^-$ decays is assumed, the limit is [22]

$$(13) \quad \mathcal{B}(B^0 \rightarrow \tau^+\tau^-) < 2.1 \times 10^{-3} \quad @ 95\% \text{ C.L.,}$$

which constitutes a factor 2.6 improvement with respect to the BaBar result [23] and is the current best limit.

REFERENCES

- [1] AAIJ R. *et al.*, *JHEP*, **02** (2016) 104, arXiv:1512.04442.
- [2] ATLAS COLLABORATION, ATLAS-CONF-2017-023.
- [3] CMS COLLABORATION, CMS-PAS-BPH-15-008.
- [4] AAIJ R. *et al.*, *Phys. Rev. Lett.*, **113** (2014) 151601, arXiv:1406.6482.
- [5] AAIJ R. *et al.*, *JHEP*, **06** (2014) 133, arXiv:1403.8044.
- [6] AAIJ R. *et al.*, *JHEP*, **09** (2015) 179, arXiv:1506.08777.
- [7] AAIJ R. *et al.*, *JHEP*, **11** (2016) 047, arXiv:1606.04731.
- [8] DESCOTES-GENON S. *et al.*, *JHEP*, **06** (2016) 092, arXiv:1510.04239.
- [9] HURTH T. *et al.*, *Nucl. Phys. B*, **909** (2016) 737, arXiv:1603.00865.
- [10] ALTMANNSHOFER W. *et al.*, *Eur. Phys. J. C*, **77** (2017) 377, arXiv:1703.09189.
- [11] BAILEY J. *et al.*, *Phys. Rev. D*, **93** (2016) 025026, arXiv:1509.06235.
- [12] ALTMANNSHOFER W. *et al.*, *JHEP*, **01** (2009) 019, arXiv:0811.1214.
- [13] AAIJ R. *et al.*, *Eur. Phys. J. C*, **77** (2017) 161, arXiv:1612.06764.
- [14] AAIJ R. *et al.*, *Phys. Rev. Lett.*, **110** (2013) 211801, arXiv:1303.1092.
- [15] PARK H. *et al.*, *Phys. Rev. Lett.*, **94** (2005) 021801, arXiv:hep-ex/0501014.
- [16] GULIN A. *et al.*, *Proc. Mach. Learn. Res.*, **14** (2011) 63.
- [17] AAIJ R. *et al.*, *JHEP*, **03** (2017) 001, arXiv:1611.07704.
- [18] BOBETH C. *et al.*, *Phys. Rev. Lett.*, **112** (2014) 101801, arXiv:1311.0903.
- [19] KHACHATRYAN V. *et al.*, *Nature*, **522** (2015) 68, arXiv:1411.4413.
- [20] AAIJ R. *et al.*, *Phys. Rev. Lett.*, **118** (2017) 191801, arXiv:1703.05747 (2017).
- [21] DE BRUYN K. *et al.*, *Phys. Rev. Lett.*, **109** (2012) 041801, arXiv:1204.1737.
- [22] AAIJ R. *et al.*, *Phys. Rev. Lett.*, **118** (2017) 251802, arXiv:1703.02508 (2017).
- [23] AUBERT B. *et al.*, *Phys. Rev. Lett.*, **96** (2006) 241802, arXiv:hep-ex/0511015.